Modeling rain-driven overland flow: Empirical versus analytical friction terms in the shallow water approximation

Geoffroy Kirstetter, Jie Hu, Olivier Delestre, Frédéric Darboux, Pierre-Yves Lagrée, Stéphane Popinet, José Maria Fullana, Christophe Josserand

Modeling rain-driven overland flow: empirical versus analytical friction terms in the shallow water approximation

Geoffroy Kirstetter, Jie Hu, Olivier Delestre, François Darboux, Pierre-Yves Lagrée, Stéphane Popinet, Jose-Maria Fullana, Christophe Josserand

Modeling rain-driven overland flow: empirical versus analytical friction terms in the shallow water approximation

G. Kirstetter[1,*], J. Hu[2], O. Delestre[2], F. Darboux[3], P-Y. Lagrée[1], S. Popinet[1], J.M. Fullana[1], and C. Josserand[1]

[1]Sorbonne Universités, UPMC Univ Paris 06, CNRS, UMR 7190, Institut Jean Le Rond d'Alembert, F-75005 Paris, France
[2]Laboratoire de Mathématiques J.A. Dieudonné - Polytech Nice-Sophia , Université de Nice - Sophia Antipolis, CNRS, UMR 7351, Parc Valrose, 06108 Nice cedex 02, France
[3]Inra, UR 0272, UR Science du sol, Centre de recherche Val de Loire, CS 40001, F-45075 Orléans Cedex 2, France
[*]geoffroy.kirstetter[at]upmc.fr

September 1, 2015

Abstract

Modeling and simulating overland flow fed by rainfall is a common issue in watershed surface hydrology. Modelers have to chose among various friction models when defining their simulation framework. The purpose of this work is to compare the simulation quality for the Manning, Darcy-Weisbach, and Poiseuille friction models on the simple case of a constant rain on an experimental flume. Results show that usual friction laws (Manning and Darcy-Weisbach) are not suitable for this type of flow. The Poiseuille friction model gave the best results both on the flux at the outlet and the velocity and depth profile along the flume. The calibration-free Poiseuille friction could therefore be used to model inter-rill overland flow. By decreasing the number of parameters to be calibrated, this could help improve simulation quality.

1 Introduction

The rain falling on agricultural fields produces overland flows, which lead to soil erosion ([Moss et al., 1979], [Morgan et al., 1999]), pollutant transport ([Cai et al., 2007], [Benkhaldoun et al., 2007]) and flood events downstream ([Cea et al., 2010], [An et al., 2015]). To prevent and understand these often undesirable effects, rain-induced flows have to be modeled accurately, thanks in particular to numerical simulations. As long as the flows have a horizontal length scale larger than the vertical one, the vertical velocity profile can be integrated, leading to a 2D system of

equations, called the shallow-water equations ([de Saint-Venant, 1871]). Such shallow-water equations are commonly used for modeling overland flow (*e.g.* [Smith et al., 2007]), tsunamis (*e.g.* [Popinet, 2011]), dam breaks and flood events (*e.g.* [An et al., 2015]) or river flooding (*e.g.* [Bates et al., 2010]), which are generally flows at high Reynolds numbers. Because numerical simulations of such systems play a significant role in government decision-making to prevent or control inundation risks, it is crucial to properly model the underlying physical mechanisms as well as develop accurate and validated numerical schemes.

One of the key point in the shallow-water framework is the effective friction term which depends on the assumption made for the vertical velocity profile. This friction term depends on several parameters but principally on the dynamical characteristics of the flow (*i.e.* laminar or turbulent). In general, because the flows are at high Reynolds numbers and also because of the complexity of the surface geometries involved, empirical laws are used, in particular the Darcy-Weisbach and the Manning models (see for instance [Chow, V., 1959], [Smith et al., 2007], [Viollet et al., 1998], [Chanson, 2004] and [An et al., 2015]).

However, it is important to notice that for rain-induced flow, the thin liquid films involved have small Reynolds numbers. Hence, the use of turbulent modeling is questionable, compared to the classical laminar friction term deduced from a Poiseuille velocity profile. Moreover, quantitative experiments are still rare ([Esteves et al., 2000]), underlying the need for systematic quantitative comparisons between numerical models and experimental measures.

In this paper, we focus on an "ideal rain" over a rough impermeable substrate. Experimental laboratory results are compared with numerical results of the shallow-water equations using both empirical (Darcy-Weisbach and Manning models) and a laminar friction term (Poiseuille model). We will show that in this case, the laminar version of the shallow-water equations is the suitable model for overland flows. The configuration studied is presented in the next section as well as the experimental setup. The numerical methods are described in section III, as well as validating cases. The numerical results are compared with the experimental measurements in section IV, and a general discussion is then given.

2 Materials and methods

2.1 The "ideal rain" case

The numerical simulation of the shallow-water equations are compared with experimental measures on an ideal configuration of overland flow produced by rain. Real cases in nature are complicated to model for various reasons: firstly the topography is often complex and not always well-known; then rainfall is usually not measured everywhere; finally many different physical mechanisms are imbricated in nature (rain, erosion, infiltration, *etc*). Dedicated experiments where these different effects can be isolated then need to be designed. We focus here on an ideal case of rain falling on a flat impermeable surface as shown in Fig. 1. The same experimental setup was used before to evaluate the validity of numerical schemes in [Delestre et al., 2009]. The flat topography is tilted by an angle a and a constant rain intensity equal to I ($mm.h^{-1}$) is imposed. The flume has a length $L = 4.04\ m$ (direction x) and width $l = 11.5\ cm$ (direction y),

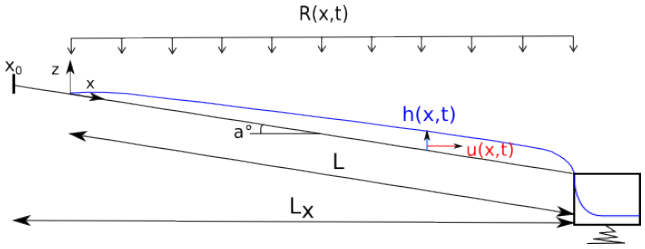

Figure 1: The "ideal rain" case: an homogeneous rain is falling on a tilted flume, producing overland flow.

and is initially dry. The rain leads to an overland flow which is characterized by $h_{2D}(x, y, t)$ the water depth and $u_{3D}(x, y, z, t)$ the velocity profile, and finally $S_0 = \tan(a)$ is the absolute value flume slope. We also define the transverse averaged water depth profile:

$$h(x,t) = \frac{1}{l}\int_{-l/2}^{l/2} h_{2D}(x,y,t)dy,$$

and the transverse and depth averaged velocity profile:

$$u(x,t) = \frac{1}{lh(x,t)}\int_{-l/2}^{l/2}\int_{0}^{h(x,t)} u_{3D}(x,y,z,t)dydz.$$

The rain intensity $R(x,t)$ is taken homogenous in space and constant during a duration t_{stop} yielding:

$$R(x,t) = \begin{cases} I & \text{if } t \in [0, t_{stop}] \\ 0 & \text{if } t > t_{stop} \end{cases} \text{ for } x \in [0, L]. \quad (1)$$

Three dynamical regimes can thus be identified on the measured outflow discharge:

- between $t = 0$ s and a time t_s, the water depth in the flume is increasing as well as the outflow discharge: it is the transient, or rising stage,
- between t_s and t_{stop} the flow is in its steady stage, and
- for $t > t_{stop}$ the rain event is finished and the outflow discharge decreases: it is the recessing stage.

This ideal configuration will be studied both experimentally and numerically in order to investigate and validate an effective rainflow overland model.

2.2 Experimental setup

2.2.1 Overall design

These experiments were carried out at the Rainfall Simulation Hall of the French Institute for Agricultural Research (INRA, Orléans, France). The test bench is a 4.04 m long and 11.5 cm wide flat flume having a rectangular section (Fig. 2). A sheet of glued printing paper is added on the flume for its hydrophilic property,

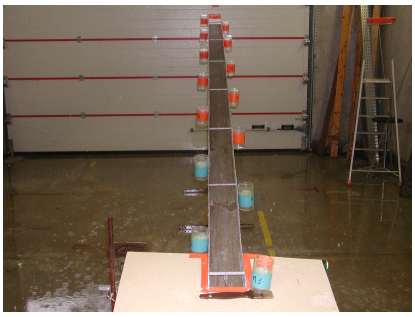

Figure 2: Front picture of the flume in the Rainfall Simulation Hall

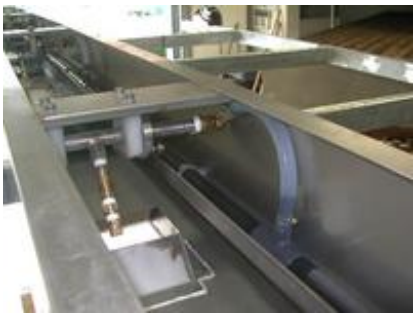

Figure 3: Picture of one oscillating nozzle above the flume

avoiding the formation of threaded flow. The varying parameters of this experiment are the channel slope S_0 and the rainfall intensity. The slope of the panel can be adjusted and is measured using a spirit level (accuracy: 0.5 $mm.m^{-1}$) and a stainless steel rule. The rainfall is produced by a nozzle-type rainfall simulator based on the design of [Foster et al., 1979] and located above the channel (Fig. 3). Water pressure is set to 90 kPa. Five oscillating nozzles are uniformly distributed over the flume (1.1 m between them). Using a combination of nozzles with slightly varying openings (Veejet 6540, 6550 and 6560; Spraying System Corp.), a coefficient of variation limited to 8.5% for the spatial variability of the rain intensity is obtained. Before each experiment, the channel is pre-wetted. A frequency of 55 sweeps per minute is used for the prescribed 50 $mm.h^{-1}$ rainfall intensity (half for the 25 $mm.h^{-1}$).

The experimental cases differ based on the prescribed rainfall intensity (25 or 50 mm.h^{-1}) and slope (2% or 5%). The three cases considered thereafter are:

- 25 mm.h^{-1} and 2%,
- 25 mm.h^{-1} and 5%,
- 50 mm.h^{-1} and 2%.

2.2.2 Measurements

Outflow hydrograph The outflow discharge is recorded during the whole run, including both the rising limb of the hydrograph (at the beginning of the rainfall) and its recessing limb (after the end of the rainfall). The outflow discharge is collected in a bucket by a funnel as schematized on Fig. 1. The outlet of the funnel is custom-made to direct the water flow laterally, avoiding flow pressure to be transmitted to the scale. The cumulative weight of the bucket was recorded using an electronic scale (30 kg range, with a 1 g resolution) at a rate of about 10 Hz. The outflow discharge measurement is replicated six times. The hydrographs (*i.e.* the derivative of the cumulative weight) are quite noisy because of the high measurement frequency for a small weight increment (maximum flow rate of about 7 $g.s^{-1}$). To make the outflow hydrograph data more readily usable, they are processed by first calculating a moving average over two seconds

on each replicate. This duration is long enough to reduce the noise while still being much shorter than the durations of the rising or recessing limbs (which are of several minutes). Then, the median values over the replicates are taken and a Kalman filter (see for instance [Kalman, 1960]) is applied to smooth the hydrograph.

Rain intensity During the experimental runs, rainfall intensity are measured by two independent methods:

- using a set of fourteen beakers positioned along the channel sides and weighted before and after the run,
- using the flow discharge at steady-state.

Depth and velocity Flow depth and velocity are measured at the middle of the flume width at steady state at up to seven positions along the channel, during one of the replicates. Flow depths are measured using a dial indicator by taking the difference between the reading at the bottom and at the surface. Each flow depth measurement is replicated twice. Flow velocities are measured with the automated salt-tracing gauge described in [Planchon et al., 2005] using a salt gauge with a 3 cm spacing between the upstream and downstream electrodes. The measurement is carried out for a few minutes at each location, with one reading every ten seconds. We compute the standard deviation of each set of measurements.

2.3 Numerical method

2.3.1 Leading equations

As stated above overland flows are well-described by the Saint-Venant equations, introduced in [de Saint-Venant, 1871], known also as the non-linear shallow-water equations. These equations are deduced by averaging the Navier-Stokes equations over the water depth, assuming horizontal length scales much larger than the vertical one. In the "ideal rain" case considered here, the 1D system of Saint-Venant is strictly equivalent of the 2D one because:

- the topography is constant over the flume width, and
- the friction on the walls are not described by the equations.

Neglecting the influence of drop impacts on the momentum, the resulting 1D equations of mass and momentum conservation are:

$$\partial_t h(x,t) + \partial_x q(x,t) = R(x,t), \tag{2}$$

$$\partial_t q(x,t) + \partial_x \Big(\frac{q(x,t)^2}{h(x,t)} + \frac{g}{2} h(x,t)^2 \Big) = g h(x,t)(S_0 - S_f), \tag{3}$$

where $h(x,t)$ and $q(x,t)$ are respectively the local flow depth and the local depth-averaged flux, $R(x,t)$ the rainfall intensity, g the acceleration of gravity, $S_0 = -\partial_x Z_b$ the opposite of the slope (with Z_b the topography) and S_f the friction coefficient in its kinematic form. The derivation of the Saint-Venant equations with rain as the first numerical simulations using this system can be

found in [Zhang and Cundy, 1989]. We define the Reynolds number Re with respect to the experimental conditions:

$$Re = \frac{\cos(a) I L}{\nu}, \tag{4}$$

which characterizes the behavior of the fluid : laminar (resp. turbulent) for $Re < 500$ (resp. $Re > 2000$), where ν is the kinematic viscosity of the fluid (typically $10^{-6} m^2.s^{-1}$ for water) and a is the angle of the flume with the horizontal. We also introduce the Froude number Fr which characterizes the relative speed of the surface waves in the flow. The flow is sub-critical (resp. supercritical) when the liquid velocity is slower (resp. faster) than the surface waves, for $Fr < 1$ (resp. $Fr > 1$). The local Froude number is:

$$Fr = \frac{u(x,t)}{\sqrt{g h(x,t)}}. \tag{5}$$

Different friction terms have been proposed in the literature depending on the flow properties. We will consider here the three main friction models: the Darcy-Weisbach model (*e.g.* [Darcy, 1857]), the Manning model (see for instances [Gauckler, 1867] and [Manning et al., 1890]), and the Poiseuille model (*e.g.* [Igawaki, 1955]). The Darcy-Weisbach and Manning models were empirically deduced while the Poiseuille model was obtained analytically. The Darcy-Weisbach model was initially designed for turbulent flows inside pipes. The friction coefficient can be written in kinematic form as:

$$S_f^{DW} = \frac{f}{8g} \frac{q(x,t)\,|q(x,t)|}{h(x,t)^3}, \tag{6}$$

where f is the Darcy-Weisbach coefficient. The Manning model was designed for open channel flows driven by gravity. The friction coefficient follows:

$$S_f^{M} = n^2 \frac{q(x,t)\,|q(x,t)|}{h(x,t)^{10/3}}, \tag{7}$$

where n is the Manning coefficient.
For a laminar flow, the vertical velocity profile is given by a Poiseuille flow. Denoting $u_{2D}(x,z,t)$ the 2D local velocity for a 2D Poiseuille flow and

$$u(x,t) = \frac{1}{h(x,t)} \int_{Z_b}^{h(x,t)} u_{2D}(x,z,t) dz$$

the local depth-averaged horizontal velocity, we can express the 2D local velocity as:

$$u_{2D}(x,z,t) = \frac{3}{2} \frac{u(x,t)}{h^2(x,t)} z(2h(x,t) - z). \tag{8}$$

An analytical solution of the Poiseuille coefficient S_f^P, without any free parameter, can be then deduced from the Navier-Stokes equations:

$$S_f^P = \frac{\nu}{g h(x,t)} \partial_z u_{2D}(x, z=0, t) = \frac{3\nu}{g} \frac{q(x,t)}{h^3(x,t)}. \tag{9}$$

Note that in contrast with the Darcy-Weisbach and Manning models, the Poiseuille friction model does not contain any empirical/adjustable parameter (other than the fluid viscosity which is set to that of water for the case of an ideal rain).

In this paper, the goal is to compare the numerical simulations for each friction term in the case of the "ideal rain" performed in the laboratory, in order to determine the best friction model in this configuration.

2.3.2 Numerical scheme

The shallow-water equations ((2) and (3)) can be written in conservative, vector form as

$$\frac{\partial}{\partial t}U(h,q) + \frac{\partial}{\partial x}F(h,q) = S(h,q,\cdot) \tag{10}$$

where $U = \begin{pmatrix} h \\ q \end{pmatrix}$ is the vector of the conserved variables, $F = \begin{pmatrix} q \\ \frac{q^2}{h} + \frac{g}{2}h^2 \end{pmatrix}$ the flux and S the source terms. In the following two different free codes will be used: Basilisk (http://basilisk.fr) and FullSWOF_1D version 1.01.01 ([Delestre et al., 2014]). Both codes are based on a similar finite-volume approach. FullSWOF_1D is especially designed to solve this kind of hydrological system, and is already including the friction terms for Darcy-Weisbach and Manning models. Moreover it has already been validated on experimental data. On the other hand, Basilisk is used to implement the friction coefficient of Poiseuille for its simplicity.

Time is discretized with time-step Δt and space with Δx, and we define $x_i = i\Delta x$ and $t_n = n\Delta t$. In the following U_i^n will refer to the vector $U = \begin{pmatrix} h(x_i,t_n) \\ q(x_i,t_n) \end{pmatrix}$. The basic Finite Volume cell is defined over the interval $]x_i - \frac{\Delta x}{2}, x_i + \frac{\Delta x}{2}[$ and will be referred to as the cell i. For the spatial reconstruction over the cell we use a MUSCL-type spatial reconstruction for the left and right states (denoted by l and r subscripts) of h,u and Z_b where Z_b stands for the topography.

We use the hydrostatic reconstruction scheme (*e.g.* [Audusse et al., 2004] and) upgraded at second order in [Audusse and Bristeau, 2005] , which (i) conserves lake-at-rest state ($h+Z_b$ constant and $u = 0$). Since [Bermudez and Vasquez, 1994], it is well known that the pressure term and the topography term need to be balanced in order to preserve at least these steady states at rest. Schemes having such property are said to be well-balanced (term introduced in [Greenberg and LeRoux, 1996]). The hydrostatic reconstruction also (ii) preserves positivity of water height, which is an important property when water layer is very thin and near wet/dry interfaces. Replacing Z_b by z for legibility, the scheme can be written as:

$$\begin{aligned} z_{i+1/2} &= max(z_{i,r}, z_{i+1,l}), \\ h_{i+1/2L} &= max(h_{i,r} + z_{i,r} - z_{i+1/2}, 0), \\ h_{i+1/2R} &= max(h_{i+1,l} + z_{i+1,l} - z_{i+1/2}, 0). \end{aligned}$$

The vector field U is defined at each side of boundaries as:

$$U_{i+1/2L} = \begin{pmatrix} h_{i+1/2L} \\ h_{i+1/2L}u_{i,r} \end{pmatrix},$$

$$U_{i+1/2R} = \begin{pmatrix} h_{i+1/2R} \\ h_{i+1/2R}u_{i+1,l} \end{pmatrix}.$$

For ensuring the balance of the volume, the scheme is written as:

$$\frac{\partial}{\partial t}U_i + \Psi(U) = S_i, \tag{11}$$

where $S_i = \begin{pmatrix} R(x,t) \\ -gh_iS_f \end{pmatrix}$ gathers the source terms. The operator $\Psi(U)$ is defined as follows:

$$\begin{aligned} \Delta x \times \Psi(U) = &\left(\mathscr{F}\left(U_{i+1/2L}, U_{i+1/2R}\right) + \frac{g}{2}\begin{pmatrix} 0 \\ h_{i,r}^2 - h_{i+1/2L}^2 \end{pmatrix}\right) \\ &- \left(\mathscr{F}\left(U_{i-1/2L}, U_{i-1/2R}\right) + \frac{g}{2}\begin{pmatrix} 0 \\ h_{i,l}^2 - h_{i-1/2R}^2 \end{pmatrix}\right) - S_{ci}, \end{aligned} \tag{12}$$

where $\mathscr{F}$ is the numerical flux, an approximation of the flux F which depends on the Riemann solver, and where the source term S_{ci} is

$$S_{ci} = \frac{g}{2}\begin{pmatrix} 0 \\ (h_{i,l} + h_{i,r})(z_{i,l} - z_{i,r}) \end{pmatrix}. \tag{13}$$

Basilisk For the code Basilisk, we chose the central-upwind scheme solver developed by [Kurganov and Levy, 2002] as approximate Riemann solver, which use a MUSCL-type reconstruction on space with a generalized minmod limiter where $\theta = 1.3$ (*e.g.* [Van Leer, 1997] and [Kurganov and Petrova, 2007]). We use a predictor-corrector scheme as time-stepping and we use a time-splitted method to deal with the source terms. As recommended in a previous study of [Delestre et al., 2009], we treat the friction source term semi-implicitly as described in the *semi-implicit scheme* paragraph. Finally, the entire scheme can be summarized as:

- Step 1 - Solving Saint-Venant system: $U_*^{n+1/2} = U^n + \frac{\Delta t}{2}\Psi(U^n)$.
- Step 2 - Computing source terms: $U^{n+1/2} = U_*^{n+1/2} + \frac{\Delta t}{2}S(U_*^{n+1/2})$.
- Step 3 - Solving Saint-Venant: $U_*^{n+1} = U^n + \Delta t \times \Psi(U^{n+1/2})$.
- Step 4 - Computing source terms: $U^{n+1} = U_*^{n+1} + \Delta t \times S(U_*^{n+1})$.

FullSWOF_1D For the code FullSWOF_1D, we chose the HLL numerical flux introduced by [Toro et al., 1994] as approximate Riemann solver, which is using a MUSCL-type reconstruction with a minmod limiter ensuring second-order in space. We use the Heun's method as time-stepping scheme, which is at second-order in time and we also use a time-splitted method to deal with source terms. The friction term is treated semi-implicitly as explained in the next paragraph. Finally, the scheme can be summarized as:

- Step 1 - Solving Saint-Venant system: $U_*^{n+1} = U^n + \Delta t \times \Psi(U^n)$.
- Step 2 - Computing source terms: $\tilde{U}^{n+1} = U_*^{n+1} + \Delta t \times S(U_*^{n+1})$.
- Step 3 - Solving Saint-Venant system: $U_*^{n+2} = U^{\tilde{n+1}} + \Delta t \times \Psi(\tilde{U}^{n+1})$.
- Step 4 - Computing the source terms: $\tilde{U}^{n+2} = U_*^{n+2} + \Delta t \times S(U_*^{n+2})$.

- Step 5: Update using Heun's method: $U^{n+1} = \dfrac{U^n + \tilde{U}^{n+2}}{2}$.

Semi-implicit scheme In both codes, we chose to treat the friction term in a semi-implicit way. This ensure the positivity of the water depth ($h > 0$) and the conservation of equilibrium states, as mentioned in [Marche, 2005] and in [Bristeau and Coussin, 2001]. We write $U_*^{n+j} = \begin{pmatrix} h_*^{n+j} \\ u_*^{n+j} h_*^{n+j} \end{pmatrix}$ with $j = \{\frac{1}{2}, 1, 2\}$ the intermediary solution before computing the source terms and we denote $U^{n+j} = \begin{pmatrix} h^{n+j} \\ u^{n+j} h^{n+j} \end{pmatrix}$ the solution after computing the source terms. Forgetting the $n+j$ index for the sake of clarity, we can write the semi-implicit scheme as follows, for instance for the Manning friction term:

$$q = \frac{q_*}{1 + \Delta t g n^2 \dfrac{|u_*| q}{h_*^{4/3}}}. \tag{14}$$

We transform equation (14) in an explicit form. Finally, the source term is $S(U_*) = \begin{pmatrix} R \\ S_q(U_*) \end{pmatrix}$ with $S_q(U_*)$:

$$S_q(U_*) = \begin{cases} -q_* \left(\dfrac{1}{\dfrac{h_*^2}{3\nu} + \Delta t} \right) & \text{for Poiseuille,} \\ -q_* \left(\dfrac{\dfrac{f|u_*|}{8h_*}}{1 + \Delta t \dfrac{f|u_*|}{8h_*}} \right) & \text{for Darcy-Weisbach,} \\ -q_* \left(\dfrac{\dfrac{g n^2 |u_*|}{h_*^{4/3}}}{1 + \Delta t \dfrac{g n^2 |u_*|}{h_*^{4/3}}} \right) & \text{for Manning,} \end{cases} \tag{15}$$

2.3.3 Numerical cases

We simulate a one dimension channel with a fixed slope S_0, as presented in Fig 1. Its horizontal length is $L_x = \frac{L+1}{\sqrt{1+S_0^2}}$ with $L = 4.04\ m$ and we shift the origin at $X = -1\ m$ to avoid effects of the rain source term at the left boundary. We set a closed boundary condition at the left of the slope ($X = -1\ m$) and a free outflow condition at the right ($X = 4.04\ m$). The rain source is equal to zero for $X < 0$ and equal to (1) for $X > 0$. For both softwares, we chose a reasonably small cell size: $\Delta x = \frac{L_x}{4096} \simeq 0.0012\ m$ for Basilisk and $\Delta x = \frac{L_x}{2000} \simeq 0.0025\ m$ for FullSWOF_1D. For both softwares, the largest time step verifying the CFL is automatically chosen. We start the simulation at $t_{start} = 0$ and we stop it at $t_{end} = 1000\ s$. The rain is stopped at $t_{stop} = 600\ s$.

The first stage was to ensure the convergence of the numerical schemes. Simulations using the case "$I = 25\text{mm.h}^{-1}$ and $S_0 = 5\%$" with different numbers of

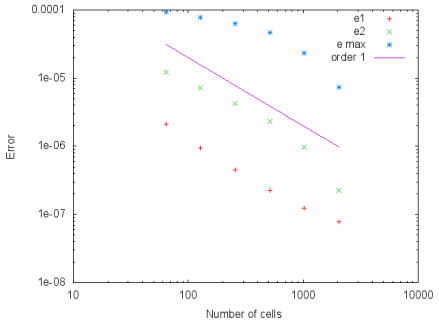

Figure 4: Relative error norms with respect to the number of cells of the simulation calculated for the case "$I = 25\text{mm.h}^{-1}$ and $S_0 = 5\%$" for the Poiseuille friction term computed with Basilisk. (logscale)

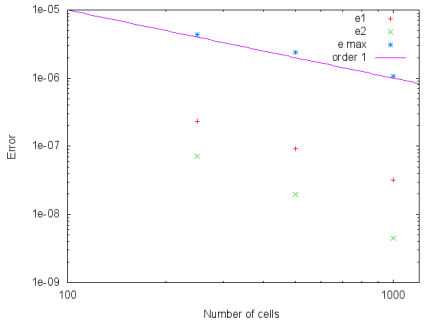

Figure 5: Relative error norms with respect to the number of cells of the simulation calculated for the case "$I = 25\text{mm.h}^{-1}$ and $S_0 = 5\%$" for the Darcy-Weisbach friction term computed with FullSWOF_1D. (logscale)

cells were performed to compute the following error norms at the steady stage (taken at $t = 599\ s$):

$$||e_1(N)|| = \frac{\int_0^L |h_N(x) - h_{max}(x)|\ dx}{L}, \tag{16}$$

$$||e_2(N)|| = \frac{\int_0^L \sqrt{(h_N(x) - h_{max}(x))^2}\ dx}{L}, \tag{17}$$

$$||e_{max}(N)|| = max_x(h_N(x) - h_{max}(x)), \tag{18}$$

with $h_N(x)$ the water depth profile with N cells and $h_{max}(x)$ the water depth profile with the maximum number of cells, respectively 4096 and 2000 for Basilisk and for FullSWOF_1D. We can see on the Fig. 4 and 5 that our simulations converged. We represent on Fig. 6 the profile of the relative error: $|h_N(x) - h_{4096}(x)|$ for different number of cells obtained for Basilisk. We can see that the maximum error is always located at the beginning of the slope. In fact, close to $X = 0$, the water depth is really small, so the hydrostatic reconstruction scheme under-estimates its value as explained in [Delestre et al., 2012]. This error is more important for larger cell-sizes. A similar result was observed with FullSWOF_1D (results not shown).

The second stage was to prescribed the parameters of the three friction terms. For the Poiseuille friction term, the typical kinematic viscosity $\nu = 10^{-6}\ m^2.s^{-1}$ (water) was considered. As described above, the Poiseuille friction coefficient do not include any calibrated value. For the Manning and Darcy-Weisbach coefficients, a calibration was performed on the experimental case "$I = 50\text{mm.h}^{-1}$ and $S_0 = 2\%$". The best possible fit was assessed by trial-and-error. This led to Manning and Darcy-Weisbach coefficients of $n = 0.025\ s.m^{-1/3}$ and $f = 0.5$ respectively. Thereafter, these values are used for the two other experimental cases as there is no reason to alter these coefficients in relation with a change in rainfall intensity or slope.

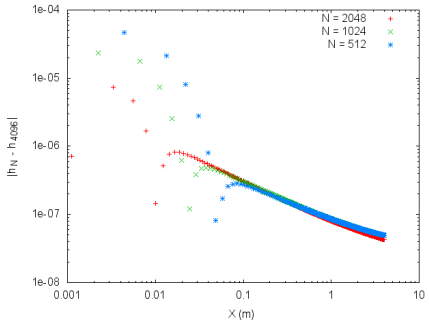

Figure 6: Profile of the relative error $|h_N(x) - h_{4096}(x)|$ during the steady stage for different number of cells N for the case "$I = 25\text{mm.h}^{-1}$ and $S_0 = 5\%$" and considering the Poiseuille friction term, computed with Basilisk. (logscale)

Tar. Rain ($mm.h^{-1}$)	Slope (%)	Num. Rain ($mm.h^{-1}$)	Reynolds	Froude	Exp. Outflow ($g.s^{-1}$)
25	2	22	24	0.4	2.8
25	5	23.5	26	0.65	3.0
50	2	45.5	50	0.6	5.8

Table 1: Main quantities for each studied case.

3 Results and discussion

The parameters relevant to each case are summarized in the Table 1. For the numerical cases, the rain intensity ($Num.\ rain$) was chosen to fit the experimental outflow during the steady stage. We also list the values of the Reynolds number and the Froude number computed numerically with the Poiseuille friction term during the steady stage ($t = 599\ s$) at the bottom of the slope ($X = 4.04\ m$). Note that the Reynolds number depends only on the experimental conditions. We can see that the flows are always laminar and subcritical. The *"Exp. Outflow"* entry in the table is the mean of the discharge measured at the end of the slope during the steady stage for the experimental cases.

3.1 Hydrographs

We compute numerically the flow rates at the bottom of the slope for the three different friction terms for a channel width of 0.115 meter filled with water and we compare them to the experimental measurements. The resulting hydrographs for each case are shown on Fig. 7.

To illustrate the dynamics of the rising limb, we define two times

- t_b as the time when the hydrograph reaches 1/10 of the steady value q_s, and

Rain and Slope	Num. or Exp. Cases	t_b (s)	t_s (s)
25 $mm.h^{-1}$ and 2 %	Exp.	55	115
	Poiseuille	55	120
	Darcy-W.	25	100
	Manning	30	105
50 $mm.h^{-1}$ and 2 %	Exp.	30	75
	Poiseuille	35	75
	Darcy-W.	15	80
	Manning	20	80
25 $mm.h^{-1}$ and 5 %	Exp.	45	85
	Poiseuille	40	85
	Darcy-W.	15	70
	Manning	20	75

Table 2: Values of t_b and t_s in each case.

- t_s as the time when hydrograph reaches its first local maximum

We note on Fig. 7(c) the times t_b and t_s for the experimental case. It is clear that t_b can be considered as the starting time of the rising limb of the hydrograph, and t_s as the beginning of the steady stage. We report on Table 2 the values of t_b and t_s for each friction term in numerical simulations and for the experimental hydrographs. For the starting time t_b, the simulations using the Darcy-Weisbach and Manning terms lead to values much smaller than the experimental value in all cases, while the simulations using the Poiseuille coefficient are much closer. For the beginning of the steady stage t_s, the simulations using the Darcy-Weisbach and Manning terms lead to values smaller than expected for the cases "$I = 25\text{mm.h}^{-1}$ and $S_0 = 2\%$" and "$I = 25\text{mm.h}^{-1}$ and $S_0 = 5\%$", and to values slightly too high for the case "$I = 50\text{mm.h}^{-1}$ and $S_0 = 2\%$". Simulations using the Poiseuille friction term give the closest estimate of t_s for the three experimental cases. Hence, it is clear that the Poiseuille friction term is the best to model the dynamic of the rising stage. Basically, the Manning and Darcy-Weisbach terms lead to a too early initiation of the rising limb (Fig. 7).

For the steady stage ($t_s < t < t_{stop}$), the experimental data show small oscillations around a mean value because of the water movement in the tank collecting the water flux at the bottom of the slope. The simulated discharges for the three friction term are very close together because at the steady stage the friction terms do not affect the water flux at the outlet. They are not strictly equal because of the different spatial discretization grid used in FullSWOF_1D (Manning and Darcy-Weisbach) and in Basilisk (Poiseuille).

Focusing on the decreasing limb ($t > 600s$), we observe that, at first, the outflow for Poiseuille decreases faster than for Darcy-Weisbach and Manning. Then the outflow for Poiseuille becomes higher than for Darcy-Weisbach and Manning. However, due to the noise in the experimental hydrographs, it is not really clear which friction term is the best at modeling this stage.

3.2 Velocity and water depth

We now look to the velocity profiles for each case during the steady stage ($t = 599s$). An important methodological difference is that experimental ve-

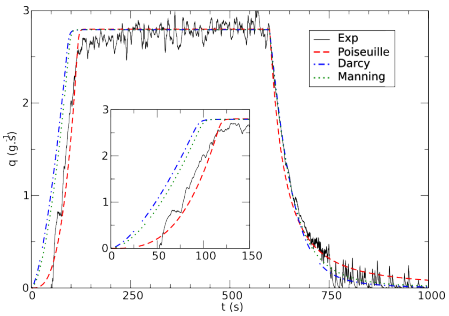

((a)) Slope = 2 %, Rain = 25 $mm.h^{-1}$

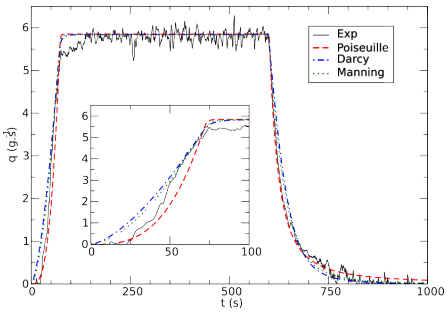

((b)) Slope = 2 %, Rain = 50 $mm.h^{-1}$

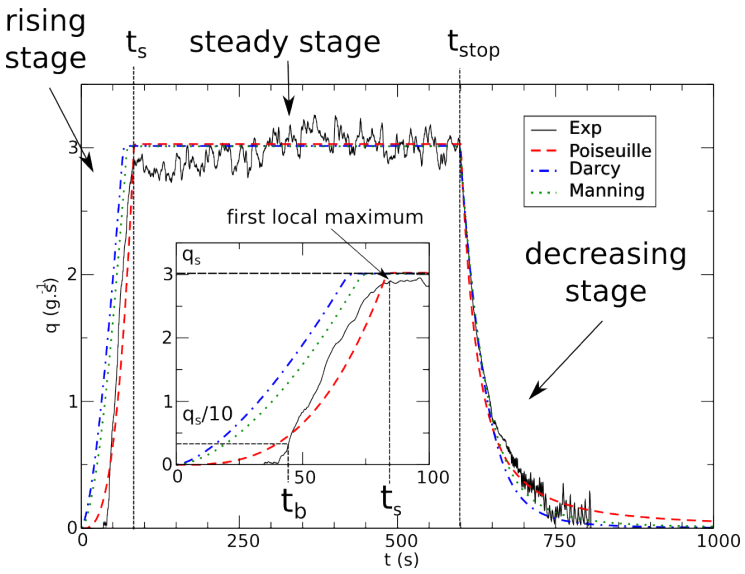

((c)) Slope = 5 %, Rain = 25 $mm.h^{-1}$. Definition of t_b, t_s, t_{stop} and the three stages of the hydrograph.

Figure 7: Numerical results with different friction terms and experimental discharge at the end of the slope versus time for different slopes and rain intensities. Zoom of the rising limb in inset.

locities are measured at the free surface in the middle of the flume, while the 1D numerical profiles can be seen as the transverse averaged values of the $3D$ field. We therefore need to perform some transformation on the velocity field before comparison. Denoting the full $3D$ local velocity field $u_{3D}(x, y, z, t)$, the 1D velocity profile computed numerically can be expressed

$$u(x,t) = \frac{1}{h(x,t)l} \int_{-l/2}^{+l/2} \int_{0}^{h(x,t)} u_{3D}(x,y,z,t) dy dz.$$

For the 3D velocity profile, we chose as hypothesis a bi-parabolic profile to take into account the influence of walls:

$$u_{3D}(x,y,z,t) = 9 \frac{u(x,t)}{h^2(x,t)l^2} (\frac{l^2}{4} - y^2) z(2h(x,t) - z). \tag{19}$$

We can finally express the experimental measurement of the velocity with respect to the 1D transverse averaged one as:

$$u_{3D}(x, y = 0, z = h(x,t), t) = \frac{9}{4} u(x,t). \tag{20}$$

We present on Fig. 8 the velocity profiles computed numerically and the mean and standard deviation of experimental measurements normalized by $\frac{9}{4}$. We can see that the normalized velocity profile is in good agreement with our numerical results independently from the friction law, validating the hypothesis made on the $3D$ velocity profiles in (19). The Manning and Darcy-Weisbach velocities are always close together and consistently too large compared to the experimental values. In all three cases, the velocities computed using the Poiseuille term are the closest to the experimental values. Hence, the Poiseuille term gives the best match for the velocity profiles.

To compare the water depth of the numerical simulations against the experimental results, we compute the averaged value of the water depth as: denoting $U_{exp}(X_{bot})$ the closest velocity measurement at the bottom of the slope ($X_{bot} = 3.72\ m$), $\overline{U}_{exp}(X_{bot})$ its transverse averaged value following (20) and $h_{exp}(X_{bot})$ the measurement of the water depth at the same coordinates. We compute the flow rates at X_{bot} as: $q_c(X_{bot}) = \overline{U}_{exp}(X_{bot}) \times h_{exp}(X_{bot})$. We can extrapolate the values at the end of the slope $q_c(L)$. During the steady stage, $\partial_t h(x,t) = 0$, then solving Equ. (2) leads to $q(x) = R \times x$, so that $q_c(L)$ is found using: $q_c(L) = q_c(X_{bot}) \times \frac{L}{X_{bot}}$. As already said, we measure the discharge at the end of the slope with the balance and we denote q_{exp} its value during the steady stage. Finally, we normalize the field h_{exp} by a factor: $\frac{q_{exp}}{q_c(L)}$ to find the transverse averaged water depth. With this method, we can extrapolate directly the water depth profile as long as the averaged velocity profile is correct. For the water depth profiles (Fig. 8), the Manning and Darcy-Weisbach terms lead to values too low. As for the velocities, the graph comparison show that the Poiseuille term gives the best match for all three cases.

To make a quantitative assessment of the numerical results, we define for each friction model a water depth index I_h and a velocity index I_u as follows:

$$I_h = \frac{1}{N} \Sigma_{i=1}^{N} \frac{\sqrt{(h_{num}(X_i) - h_{exp}(X_i))^2}}{h_{exp}(X_i)}, \tag{21}$$

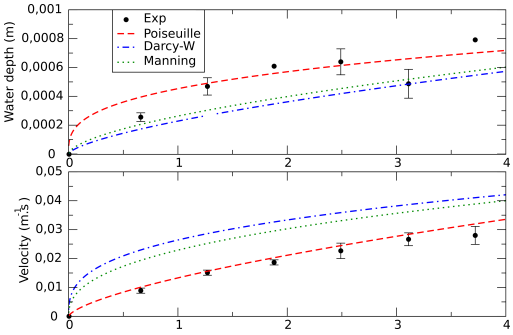

((a)) Slope = 2 %, Rain = 25 $mm.h^{-1}$

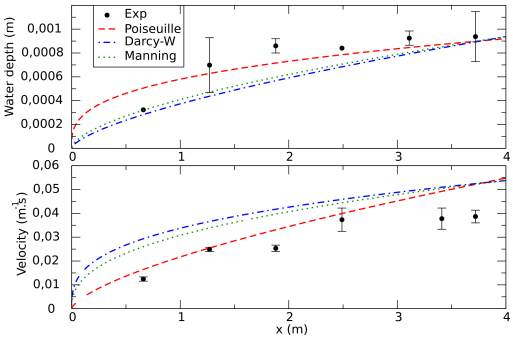

((b)) Slope = 2 %, Rain = 50 $mm.h^{-1}$

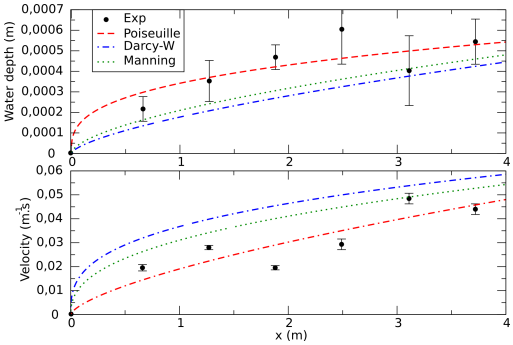

((c)) Slope = 5 %, Rain = 25 $mm.h^{-1}$

Figure 8: Water depth (top) and velocity (bottom) profiles along the slope at the steady stage ($t = 599$ s). Error bars are standard errors.

Rain and Slope	Friction model	I_h	I_u
25 $mm.h^{-1}$ and 2 %	Poiseuille	0.20	0.09
	Darcy-W.	0.31	0.79
	Manning	0.28	0.61
50 $mm.h^{-1}$ and 2 %	Poiseuille	0.17	0.22
	Darcy-W.	0.21	0.56
	Manning	0.17	0.47
25 $mm.h^{-1}$ and 5 %	Poiseuille	0.17	0.23
	Darcy-W.	0.34	0.55
	Manning	0.25	0.37

Table 3: Values of I_h and I_u in each case. The closer to zero the index is, the closer to the experimental measurements the simulation is.

$$I_u = \frac{1}{N}\Sigma_{i=1}^{N}\frac{\sqrt{(u_{num}(X_i) - u_{exp}(X_i))^2}}{u_{exp}(X_i)}, \tag{22}$$

with $N = 6$ the number of experimental measurements, X_i the position on the flume of the experimental measurements, h_{num} and u_{num} the numerical results for the water depth and the velocity, respectively, at the position X_i for the corresponding friction model (Darcy-Weisbach, Manning or Poiseuille) and h_{exp} and u_{exp} the mean of the water depth and velocity, respectively, measured experimentally at the position X_i. A zero value for these indexes means that the numerical result fits perfectly the experimental measurements.

For the water height, the index is the smallest when the Poiseuille term is used (Table 3). The Darcy-Weisbach term leads to the highest values. Only in the case "$I = 50\text{mm.h}^{-1}$ and $S_0 = 2\%$" the Manning term gives a result as good as the Poiseuille term. For the velocity, the index is always the lowest with the Poiseuille term and the highest for the Darcy-Weisbach term. Hence, it is clear that the Poiseuille friction term is the best to model both the water depth and the velocity profiles at steady state.

Overall, for a smooth surface with a rain-fed, laminar and subcritical flow, the Poiseuille term leads consistently to the best match for the water flux at the outlet during the initiation of the hydrograph, for the water depth profile at steady state and for the velocity profile at steady state. Hence, the Poiseuille term could be used for inter-rill overland flow, a condition commonly encountered in watershed surface hydrology. The adequacy of this term should now be evaluated on field data.

Compared to the empirical Manning and Darcy-Weishbach terms, the Poiseuille term has the advantage to be defined analytically and to have no parameter to be calibrated. In watershed surface hydrology, issues of over-calibration, *i.e.* the use of codes requiring the calibration of numerous parameters based on limited data set, have been leading to equifinality cases and to a limited confidence in the simulation quality [Beven, 2008]. The use of the Poiseuille term could help in achieving a parsimonious parametrization [Gong et al., 2011], improving the overall quality of hydrologic simulations.

4 Conclusion

Three different friction terms in the Saint-Venant equations have been examined: the commonly used Darcy-Weisbach and Manning models which are empirical and the Poiseuille term, which is deduced directly from the laminar Navier-Stokes equations. This last friction term does not depend on any free parameter (aside from the fluid viscosity). The "ideal rain" case has been reproduced in laboratory and numerical simulations of these events have been performed for these friction terms with the open-source codes Basilisk and FullSWOF_1D. The simulation results have been compared with the experimental results. For both the discharge at the end of the flume and for the velocity and water depth profiles along the flume, we have shown that the Poiseuille friction term appears to be the most relevant to reproduce such laboratory experiments. We recommend evaluating the Poiseuille friction term on inter-rill overland flow cases measured in the field. If suitable, this would reduce the number of parameters to be calibrated, leading to an increase in simulation quality.

5 Acknowledgment

The Axa Research Fund is thanked for its financial support through a JRI grant. The experimental work was supported by the ANR project METHODE #ANR-07-BLAN-0232 and was carried out by Loïc Prud'homme and Bernard Renaux, who are thanked for their technical skills.

References

[An et al., 2015] An, H., Yu, S., Lee, G., and Kim, Y. (2015). Analysis of an open source quadtree grid shallow water flow solver for flood simulation. *Quaternary International*, pages 1–11.

[Audusse et al., 2004] Audusse, E., Bouchut, F., Bristeau, M.-O., Klein, R., and Perthame, B. (2004). A Fast and Stable Well-Balanced Scheme with Hydrostatic Reconstruction for Shallow Water Flows. *SIAM Journal on Scientific Computing*, 25(6):2050–2065.

[Audusse and Bristeau, 2005] Audusse, E. and Bristeau, M.-o. (2005). A 2d Well-balanced Positivity Preserving Second Order Scheme for Shallow Water Flows on Unstructured Meshes. *Journal of Computational Physics*, 206(1):311–333.

[Bates et al., 2010] Bates, P. D., Horritt, M. S., and Fewtrell, T. J. (2010). A simple inertial formulation of the shallow water equations for efficient two-dimensional flood inundation modelling. *Journal of Hydrology*, 387(1-2):33–45.

[Benkhaldoun et al., 2007] Benkhaldoun, F., Elmahi, I., and Seaïd, M. (2007). Well-balanced finite volume schemes for pollutant transport by shallow water equations on unstructured meshes. *Journal of Computational Physics*, 226(1):180–203.

[Bermudez and Vasquez, 1994] Bermudez, A. and Vasquez, E. (1994). upwind methods for hyperbolic conservation laws with source terms. *Computers Fluids*, 23(8):1049–1071.

[Beven, 2008] Beven, K. (2008). On doing better hydrological science. *Hydrological processes*, 22(November 2008):3549–3553.

[Bristeau and Coussin, 2001] Bristeau, M.-O. and Coussin, B. (2001). Boundary Conditions for the Shallow Water Equations solved by Kinetic Schemes. Technical Report RR-4282, INRIA.

[Cai et al., 2007] Cai, L., Xie, W. X., Feng, J. H., and Zhou, J. (2007). Computations of transport of pollutant in shallow water. *Applied Mathematical Modelling*, 31(3):490–498.

[Cea et al., 2010] Cea, L., Garrido, M., and Puertas, J. (2010). Experimental validation of two-dimensional depth-averaged models for forecasting rainfall-runoff from precipitation data in urban areas. *Journal of Hydrology*, 382(1-4):88–102.

[Chanson, 2004] Chanson, H. (2004). *The hydraulics of open channel flow : an introduction, second edition.* Butterworth-Heinemann, Oxford, second edition.

[Chow, V., 1959] Chow, V., T. (1959). *Open channel flow.* MacGraw-Hill Book Co. Inc., New-York.

[Darcy, 1857] Darcy, H. (1857). *Recherches expérimentales relatives au mouvement de l'eau dans les tuyaux (Vol. 1).* Mallet-Bachelier.

[de Saint-Venant, 1871] de Saint-Venant, A. B. (1871). Théorie du mouvement non permanent des eaux, avec application aux crues des rivières et à l'introduction des marées dans leurs lit. *Comptes Rendus des séances de l'Académie des Sciences*, 73:237–240.

[Delestre et al., 2014] Delestre, O., Cordier, S., Darboux, F., Du, M., James, F., Laguerre, C., and Planchon, O. (2014). FullSWOF : a software for overland flow simulation. *In Advances in Hydroinformatics*, pages 221–231.

[Delestre et al., 2012] Delestre, O., Cordier, S., Darboux, F., and James, F. (2012). A limitation of the hydrostatic reconstruction technique for Shallow Water equations. *Comptes Rendus Mathematique*, 350(13-14):677–681.

[Delestre et al., 2009] Delestre, O., Cordier, S., James, F., and Darboux, F. (2009). Simulation of Rain-Water Overland-Flow. In *Proceedings of the 12th international conference on Hyperbolic Problems, University of Maryland*, pages 1–11, College Park (USA).

[Esteves et al., 2000] Esteves, M., Faucher, X., Galle, S., and Vauclin, M. (2000). Overland flow and infiltration modelling for small plots during unsteady rain: Numerical results versus observed values. *Journal of Hydrology*, 228(3-4):265–282.

[Foster et al., 1979] Foster, G., Eppert, F., and Meyer, L. (1979). A programmable rainfall simulator for field plots. In *Proceedings of Rainfall Simulator Workshop*, pages 45—-59.

[Gauckler, 1867] Gauckler, P. (1867). Etudes Théoriques et Pratiques sur l'Ecoulement et le Mouvement des Eaux. Technical report, Gauthier-Villars, Paris.

[Gong et al., 2011] Gong, L., Halldin, S., and Xu, C. Y. (2011). Large-scale runoff generation - Parsimonious parameterisation using high-resolution topography. *Hydrology and Earth System Sciences*, 15(8):2481–2494.

[Greenberg and LeRoux, 1996] Greenberg, J. M. and LeRoux, a. Y. (1996). A Well-Balanced Scheme for the Numerical Processing of Source Terms in Hyperbolic Equations. *SIAM Journal on Numerical Analysis*, 33(1):1–16.

[Igawaki, 1955] Igawaki, Y. K. U. (1955). Fundamental studies on the runoff analysis by characteristic. *Disaster prevention research institute*, December(10):1–29.

[Kalman, 1960] Kalman, R. E. (1960). A New Approach to Linear Filtering and Prediction Problems. *Transactions of the ASME-Journal of Basic Engineering*, 82(Series D):35–45.

[Kurganov and Levy, 2002] Kurganov, A. and Levy, D. (2002). Central-upwind schemes for Saint-Venant system. *Mathematical modelling and numerical analysis*, 36(3):397–425.

[Kurganov and Petrova, 2007] Kurganov, A. and Petrova, G. (2007). A second-order well-balanced positivity preserving central-upwind scheme for the Saint-Venant system. *Communications in Mathematical Sciences*, 5(1):133–160.

[Manning et al., 1890] Manning, R., Griffith, J. P., Pigot, T. F., and Vernon-Harcourt, L. F. (1890). On the flow of water in open channels and pipes. *Transactions of the Institution of Civil Engineers of Ireland*, 20:161–207.

[Marche, 2005] Marche, F. (2005). *Theoretical and numerical study of shallow water models: applications to nearshore hydrodynamics.* PhD thesis, Bordeaux 1.

[Morgan et al., 1999] Morgan, R. P. C., Quinton, J. N., Smith, R. E., Govers, G., Poesen, J. W. A., Auerswald, K., Chisci, G., Torri, D., and Styczen, M. E. (1999). Discussion on 'The European soil erosion model (EUROSEM): A dynamic approach for predicting sediment transport from fields and small catchments'. *Earth Surface Processes and Landforms*, 24(6):563–565.

[Moss et al., 1979] Moss, A. J., Walker, P. H., and Hutka, J. (1979). raindrop-stimulated transportation in shallow-water flows: an experimental study. *Sedimentary geology*, 22:165–184.

[Planchon et al., 2005] Planchon, O., Silvera, N., Gimenez, R., Favis-Mortlock, David Wainwright, J., Le Bissonnais, Y., and Govers, G. (2005). An automated salt-tracing gauge for flow-velocity measurement. *Earth Surface Processes and Landforms*, 30(7):833—-844.

[Popinet, 2011] Popinet, S. (2011). Quadtree-adaptive tsunami modelling. *Ocean Dynamics*, 61(January):1261–1285.

[Smith et al., 2007] Smith, M. W., Cox, N. J., and Bracken, L. J. (2007). Applying flow resistance equations to overland flows. *Progress in Physical Geography*, 31(4):363–387.

[Toro et al., 1994] Toro, E. F., Spruce, M., and Speares, W. (1994). Restoration of the Contact Surface in the HLL {Riemann} Solver. *Shock Waves, Vol 4*, pages 25–34.

[Van Leer, 1997] Van Leer, B. (1997). Towards the Ultimate Conservative Difference Scheme. *Journal of Computational Physics*, 135(2):229–248.

[Viollet et al., 1998] Viollet, P.-L., Chabard, J.-P., Esposito, P., and Laurence, D. (1998). *Mécanique des fluides appliquée Écoulements incompressibles*. Presses de l'École Nationale des Ponts et Chaussées, Paris.

[Zhang and Cundy, 1989] Zhang, W. and Cundy, T. W. (1989). Modeling of Two-Dimensional Overland Flow. *Water Resources Research*, 25(9):2019–2035.